

See discussions, stats, and author profiles for this publication at: <https://www.researchgate.net/publication/45387460>

Epitaxial Electrodeposition of ZnO Nanowire Arrays on p-GaN for Efficient UV-Light-Emitting Diode Fabrication

ARTICLE in ACS APPLIED MATERIALS & INTERFACES · JULY 2010

Impact Factor: 6.72 · DOI: 10.1021/am100334c · Source: PubMed

CITATIONS

76

READS

101

6 AUTHORS, INCLUDING:



Lupan Oleg

University of Central Florida

136 PUBLICATIONS 3,567 CITATIONS

[SEE PROFILE](#)



Thierry Pauperté

Chimie ParisTech

163 PUBLICATIONS 4,722 CITATIONS

[SEE PROFILE](#)



Bruno Viana

École nationale supérieure de chimie de P...

386 PUBLICATIONS 5,557 CITATIONS

[SEE PROFILE](#)



Ion Tiginyanu

Academy of Sciences of Moldova

389 PUBLICATIONS 3,805 CITATIONS

[SEE PROFILE](#)

Epitaxial Electrodeposition of ZnO Nanowire Arrays on p-GaN for Efficient UV-Light-Emitting Diode Fabrication

O. Lupan,^{†,‡} T. Pauperté,^{*,†} B. Viana,[§] I. M. Tiginyanu,[⊥] V. V. Ursaki,[⊥] and R. Cortès^{||}

Laboratoire d'Electrochimie, Chimie des Interfaces et Modélisation pour l'Energie (LECIME) UMR7575, CNRS ENSCP-Chimie Paristech, 11 rue Pierre et Marie Curie, 75231 Paris, cedex 05, France, Laboratoire de Chimie de la Matière Condensée de Paris, UMR 7574, ENSCP, 11 rue P. et M. Curie, 75231 Paris cedex 05, France, Institute of Electronic Engineering and Nanotechnologies, Institute of Applied Physics, Academy of Sciences of Moldova, MD-2028 Chisinau, Republic of Moldova, and Laboratoire de Physique de la Matière Condensée, UMR 7643, Ecole Polytechnique, 91128 Palaiseau, France

ABSTRACT The electrochemical growth of ZnO nanowire arrays on p-type GaN (0001) single crystalline thin films supported on sapphire is demonstrated for the first time. The wires were directly epitaxially grown on the GaN with the relationship ZnO(0001)[10̄10]||GaN(0001)[10̄10]. By glancing-angle XRD experiments, the ZnO mosaicity was shown to be as low as 1.2°. The deposited ZnO-NWs exhibited a very low density of intrinsic defects as demonstrated by micro-Raman and photoluminescence (PL) experiments. The only significant PL emission of the heterojunction at room temperature was the near band edge one of ZnO at 382 nm. After integration of the heterostructure in a solid-state light-emitting diode device, a rectifying behavior was found with a forward current onset at 3 V. The diodes emitted an unique UV-light centered at 397 nm for either as-prepared or annealed samples. The emission threshold voltage was 4.4 V. The violet visible tail of the emission could be observed above 5–6 V with the naked eyes. The present results clearly state the remarkable quality of the electrochemical ZnO material and ZnO-NWs/p-GaN interface as well as the effectiveness of electrodeposited epitaxial ZnO as an active layer in solid-state UV-LED structure.

KEYWORDS: ZnO • UV emission • light-emitting diode structures • low voltage • epitaxy • electrodeposition

1. INTRODUCTION

Zinc oxide is a II–VI semiconductor (SC) material with a wide band gap of 3.37 eV and a large exciton binding energy of 60 meV at room temperature (1). ZnO can be grown as individual or arrays of one-dimensional nanostructures that exhibit superior and additional properties compared to bulk and thin films because of a large surface-to-volume ratio and quantum confinement effects (1, 2). The arrays of ZnO nanowires are promising for a large variety of applications in opto-electronic devices including light emitting diodes (LEDs) (2–14) and solar cells (15–17). Nanowire (NW)-based LEDs have drawn large interest because of the many advantages compared to thin-film-based devices. Marked improved performances are expected from nanostructured active layers for light emission (7, 13). Nanowires can act as direct waveguides and favor light extraction without use of lens and reflectors. Moreover, the use of wires avoids the presence of grain boundaries and

then the emission efficiency is boosted by the absence of nonradiative recombinations at the joint defects. The junctions between the n- and p-type semiconductors can also be of very high quality with low interfacial strain and defect density because of a reduced contact area between the two materials in the case of epitaxial heterojunctions.

However, ZnO is intrinsically an n-type semiconductor because of native donors and the synthesis of reproducible, stable p-type ZnO material with sufficient high conductivity and carrier concentration is still in a development phase (18–20). Typically, up to now, the performances of ZnO-based homojunction devices have remained inferior to the ZnO-based heterojunction LEDs (n-type ZnO on a p-type SC) (14). Among the various p-type SC candidates, GaN appears as the most promising since the heteroepitaxy of ZnO on GaN is facilitated by their same hexagonal wurtzite structure with a low lattice mismatch (1.9% for the a parameter) (21–24). Moreover, the two materials have a similar thermal expansion coefficient and commercial highly p-doped GaN is available. Because the growth of ZnO-NWs can be done by various techniques, a pertinent approach appears to be growing ZnO nanowire arrays on p-GaN thin films. Most of the efforts for the preparation of ZnO NW-based LED have been focused on vapor phase growths of ZnO such as MOCVD (metal organic chemical vapor deposition) (5–9) or MOVPE (metal organic vapor phase epitaxy) (25). There have been much less published works on the use of solution grown ZnO-NW based heterostructures (12–14, 26). Typi-

* Corresponding author. E-mail: thierry-pauporté@chimie-paristech.fr.

Received for review April 16, 2010 and accepted June 28, 2010

[†] UMR 7575, ENSCP-Chimie Paristech.

[‡] On leave from Department of Microelectronics and Semiconductor Devices, Technical University of Moldova, 168 Stefan cel Mare Blvd., Chisinau, MD-2004, Republic of Moldova.

[§] UMR 7574, ENSCP.

[⊥] Academy of Sciences of Moldova.

^{||} UMR 7643, Ecole Polytechnique.

DOI: 10.1021/am100334c

2010 American Chemical Society

cally, ZnO-NWs were grown by seeded hydrothermal techniques. The corresponding LED characteristics were rather disappointing with some authors reporting a violet emission peak at 410–415 nm assigned to recombination in p-GaN combined with a broad visible emission of lower intensity, the emissions being observed for bias voltages higher than 10–15 V (13, 26).

The present paper focuses on the electrochemical deposition (ECD) technique, an original low-temperature growth method from solution for the preparation of ZnO-NW based LEDs. Electrodeposition has proven to be interesting for the epitaxial growth of ZnO on *n*-GaN (21–24) and Au (27, 28). Because of the electron exchange during the growth, ECD gives rise to an excellent electrical contact between the substrate and the deposited layer and is then promising for the preparation of opto-electronic devices. In the present case ZnO nanowires were electrodeposited, in the absence of seed layer or catalyst, directly on a *p*-type GaN single crystal supported on sapphire. Arrays of epitaxially grown ZnO nanowires were produced. We have observed that the density of wire increased with the concentration of zinc ions in the deposition bath. The epitaxial growth was clearly stated by glancing angle X-ray diffraction (GA-XRD) ϕ -scan experiments for seven different families of diffraction planes. The deposited material was of high structural and optical quality with a significant improvement after thermal annealing at 300 °C and the corresponding heteroepitaxial structures have been successfully integrated in efficient UV-LED structures.

2. EXPERIMENTAL SECTION

The ZnO nanowire arrays were grown by electrodeposition according to a procedure described elsewhere (24). The substrate was a commercial magnesium-doped GaN (0001)-oriented layer grown on sapphire with the *c*-axis perpendicular to the substrate (purchased from TDI, Inc. corporation). The *p*-type GaN layer was 3 μ m thick and the dopant concentration was $3 \times 10^{18} \text{ cm}^{-3}$. The crystal miscut was 0.59°. Prior to deposition, the *p*-GaN (0001) substrate was degreased in trichloroethylene at 50 °C for 10 min, subsequently cleaned 5 min in warm acetone at 53 °C under ultrasonics and 10 min in methanol at RT under ultrasonics, and then rinsed with deionized water. In a second step, the crystal was etched 10 min in concentrated ammonia (28 %) at 60 °C (24), subsequently etched in HCl:H₂O (1:1 vol.) for 12 min to remove any native oxide (29, 30), and finally rinsed with high-purity Millipore water (resistivity of 18.2 MΩ · cm). These cleaning steps were performed just before to start the electrodeposition process. Cleaned GaN substrates were mounted on a static working electrode (WE) with a copper support. The electrical contact between the substrate and the support was taken by rubbing In–Ga eutectic. The low resistance of the contact was checked by *I*–*V* measurements. The deposition bath was an aqueous solution containing 0.07 mM (samples A), 0.10 mM (samples B), or 0.25 mM (samples C) ZnCl₂ plus 0.1 M KCl as a supporting electrolyte and saturated with O₂ (31, 32). The ZnO nanowires were grown at 85 °C for 1 h in a classical three-electrode cell (32, 33). The applied potential was –1.12 V versus the saturated calomel electrode (SCE). A platinum wire was used as a counter-electrode. The ZnO deposits were performed through a circular mask of 3 mm in diameter (0.07 cm²). After electrodeposition, the substrate was rinsed with Millipore water and dried under an Ar flux. The

Table 1. Analysis of the GA-XRD Patterns of an Epitaxial ZnO-NWs/*p*-GaN Heterojunction (sample C) for Various Families of Plane: Position of the Detector, Mean FWHM Deduced from the Six ϕ -Scan Diffraction Peaks, and Sample Mosaicity

plane family	height detector δ (deg)	detector azimuth γ (deg)	GaN fwhm (deg)	ZnO fwhm (deg)
11̄20	0	57.86	0.38	1.26
20̄20	0	67.91	0.43	1.21
10̄11	17.405	32.27	0.43	1.14
20̄21	17.46	67.93	0.42	1.09
10̄12	36.39	32.91	0.46	1.47
11̄22	36.37	62.09	0.42	1.27
20̄22	36.455	73.58	0.43	1.39
Mosaicity				
GaN				0.3°
ZnO				1.2°

ZnO/GaN heterostructure was annealed at 300 °C in air during 30 min when specified.

The sample morphologies were examined with a high-resolution Ultra 55 Zeiss FEG scanning electron microscope (SEM) at an acceleration voltage of 10 kV. X-ray diffraction patterns were recorded with a homemade four-circle apparatus operated at 35 kV and 25 mA using the CuK α radiation with $\lambda = 1.5406 \text{ \AA}$. The glancing angle (GA) between the sample and the incident beam was 0.6° in order to optimize the signal from ZnO. The Bragg conditions were obtained by setting the detector in two directions with angular coordinates in the height direction and azimuthal direction noted δ and γ respectively (Table 1). The ϕ -scan measurements were performed by rotating the sample around an axis perpendicular to the sample. The micro-Raman spectra of the ZnO-NW arrays were measured using a Horiba Jobin-Yvon LabRam IR system in a backscattering configuration. The 632.8 nm line of a He–Ne laser was used for off-resonance excitation with less than 4 mW power at the sample.

The continuous wave (cw) photoluminescence (PL) was excited by the 325 nm line of a He–Cd Melles Griot laser. The emitted light was collected by lenses and was analyzed with a double spectrometer providing a spectral resolution better than 0.5 meV. The signal was detected by a photomultiplier working in the photon counting mode. The laser power for the PL excitation was about 20 mW. The samples were mounted on the cold station of a LTS-22-C-330 optical cryogenic system. The LED device assembly was maintained by a bulldog clip and polarized with a Keitley 2400 source. Its electroluminescence (EL) was collected by an optical fiber connected to a CCD Roper Scientific detector (cooled Pixis 100 camera) coupled with a SpectraPro 2150i monochromator. The monochromator focal lens was 150 mm, grating of 300 gr/mm blazed at 500 nm in order to record the emission of the ZnO in the whole near-UV–visible range.

3. RESULTS AND DISCUSSION

The cyclic voltammogram (CV) at 85 °C of a bare *p*-GaN(001) electrode in the deposition bath containing 0.25 mM ZnCl₂ is shown in Figure 1a. A single cathodic wave appears below –0.8 V vs SCE. The wave is due to the electrochemical reduction of molecular oxygen at the electrode surface (34) and similar curves were recorded at lower ZnCl₂ concentration. The electrochemical reaction generates hydroxide ions which react with zinc ions present in the

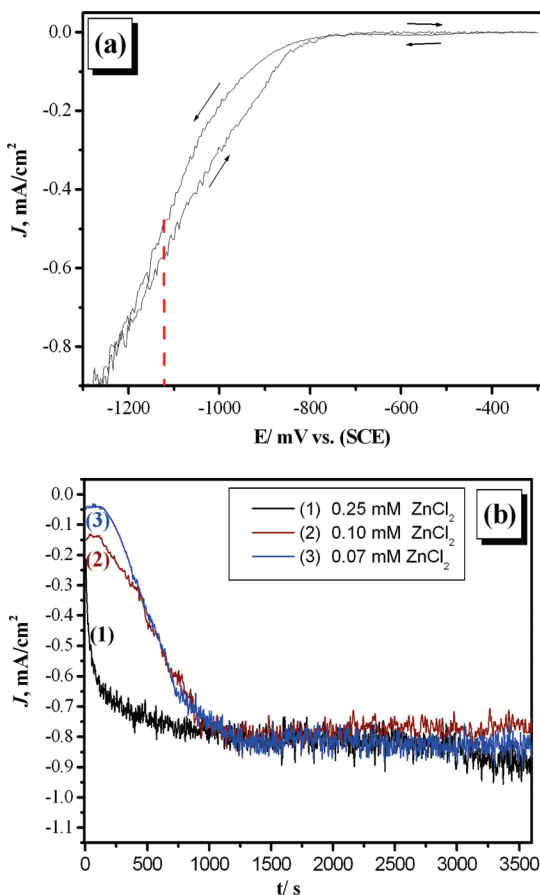


FIGURE 1. (a) Cyclic voltammogram of a bare and clean p-type GaN(0001) static electrode in a solution containing 0.25 mM ZnCl_2 and 0.1 KCl (pH 5.5) at 85 °C saturated with oxygen. The solution was stirred at 300 rpm and the sweep rate was 10 mV s⁻¹. The red dotted line marks the applied potential for ZnO electrodeposition. (b) Chronoamperograms of a static p-type GaN(0001) electrode polarized at -1.12 V vs SCE in the same bath for various ZnCl_2 content.

solution and produce an array of ZnO nanowires at the GaN surface (24, 35). We can mention that no metallic zinc was produced over the scanned potential range because no reoxidation peak could be observed on the positive-going scan of the CV curve. The ZnO layer depositions were performed at a constant applied electrochemical potential. After many tests, an applied potential of -1.12 V vs SCE was chosen in order to combine a slow growth rate which favors the material quality (36) and a good homogeneity of the deposited ZnO NW arrays. In Figure 1b shows chronopotentiograms recorded upon the growth of ZnO nanowires in baths containing various concentrations of ZnCl_2 . At high concentration, a steady state current density of -0.8 mA cm⁻² was reached rapidly. The supersaturation near the electrode was attained rapidly and the electrode was then promptly covered by the ZnO seeds. On the contrary, at lower precursor concentrations, an induction period of approximately 120s was necessary to reach the supersaturation. Then after, the deposition current increased more slowly probably due to a more progressive nucleation of the ZnO seeds. The steady-state currents were the same for the three experiments because this parameter is mainly related

to the molecular oxygen concentration in the bath, which was fixed at the saturation level in our experiments.

The role of zinc ion concentration on the ZnO nucleation has been confirmed by SEM observations of the deposited layers. In Figure 2, we can see that after 1 h of deposition time, the GaN substrates were not fully covered by a dense film of ZnO but by an array of ZnO nanowires. In the present case, the formation of nanostructured ZnO was favored by the rather high deposition temperature and the low concentration of the zinc ion precursor (36). The latter parameter induces the blocking of the lateral growth of the crystallites after a short induction time period, which is followed by a vertical growth. It has been suggested that the pH change at the interface upon deposition along with the zinc ion precursor depletion may play an important role in the growth rate of the various crystallographic planes (31). In Figure 2, we can also observe that the higher the ZnCl_2 bath concentration, the higher the density of wires. In the case of 0.25 mM ZnCl_2 , the space separating the free-standing wires was small. More material was deposited because of a higher deposition efficiency. Another interesting observation is that on the micrograph's top views the ZnO crystallites have a hexagonal shape indicating that the wires are grown along their *c*-axis in an out-of-plane orientation similar to that of the substrate. Moreover, the hexagons of the various ZnO crystallites are oriented in the same in-plane direction and then the wires are epitaxially grown (22, 24). Because of the epitaxial growth, the n-ZnO wires were perfectly vertically oriented on p-GaN as illustrated in the inset of Figure 2b. The wire length was approximately 800–900 nm regardless of the ZnCl_2 concentration and the nanowires were directly attached to the GaN film (inset Figure 2b). The SEM top-views point out some dispersion of the ZnO crystallite sizes, especially for the low precursor concentrations (0.07 mM and 0.1 mM) because the nucleation was not instantaneous but progressive.

The structural relationship between the deposited ZnO and the p-GaN substrate was investigated by four-circle XRD experiments at glancing angle (GA). GA-XRD ϕ -scans have been performed for seven different families of planes (22, 23, 37). Well-defined peaks with a 6-fold symmetry were observed in every case (Figure 3 and Figure S1 in the Supporting Information). The zoom views (see Figure 3b and Figure S1 in the Supporting Information) clearly show the presence of a second diffraction peak at the left-hand of the main one. The main one is due to the GaN single-crystal substrate and the second is assigned to electrodeposited epitaxial ZnO-NWs. The epitaxial relationship is $\text{ZnO}(0001)[\bar{1}0\bar{1}0]\parallel[\bar{0}001]\text{GaN}[10\bar{1}0]$. The near-zero value of the pattern baseline reveals that the whole ZnO is epitaxially deposited. The GaN and ZnO diffraction peaks were fitted with Gaussian curves and their fwhm have been calculated for the seven different families of plane. Examples of the good quality of the fits are shown in Figure 3b and Figure S1 in the Supporting Information. Each family of ZnO plane is characterized by the δ and γ pair of coordinates reported in Table 1. Because of the close lattice parameters of ZnO

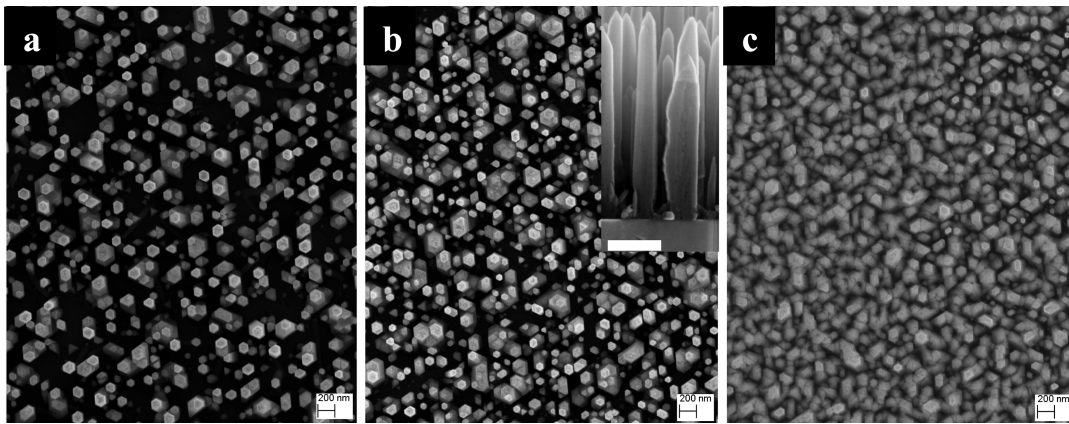


FIGURE 2. SEM top-views of the ZnO nanowires electrodeposited on p-type GaN(0001) substrate: (a) sample A (0.07 mM ZnCl₂), (b) sample B (0.10 mM ZnCl₂) (the inset is a side-view of the wires), and (c) sample C (0.25 mM ZnCl₂). The scale bars are 200 nm.

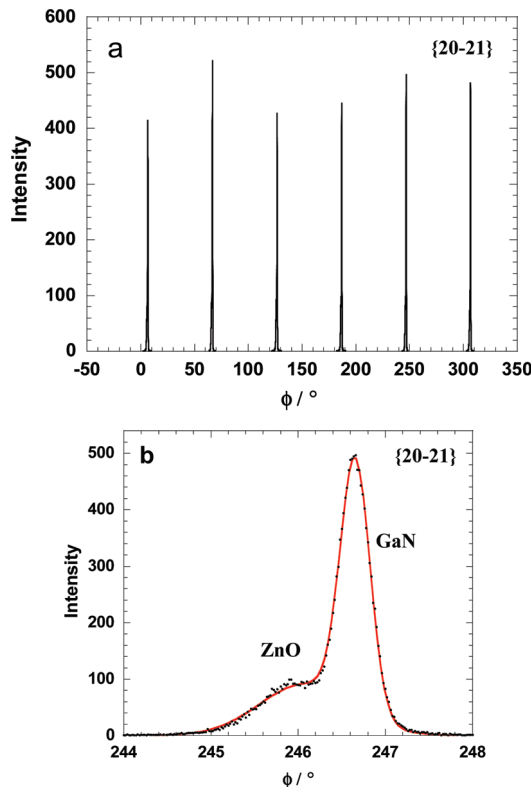


FIGURE 3. (a) GA-XRD ϕ -scan of the {20-21} family of planes for sample C. (b) Enlarged view of one of the diffraction peak: experimental points and two-Gaussian curve fit line.

and GaN, the GaN signal was always detected with the ZnO one on the ϕ -scans. Their full-width at half maximum (fwhm) have been calculated by averaging the values for the six diffraction peaks of a scan are summarized in Table 1 for the seven investigated families of planes. The fwhm of GaN ranged between 0.38 and 0.46°. The in-plane misorientation was larger for the electrodeposited ZnO and ranged between 1.09 and 1.47°. From data in Table 1, the mosaicity of GaN and ZnO have been calculated at 0.3 and 1.2° respectively (Table 1) (37). The GA-XRD analysis shows that the electrodeposited ZnO was in a very good epitaxial relationship with the substrate. We can note that the in-plane misorientation in the present case is lower than the one reported in a previous work by Pauporte et al. for dense electrodeposited

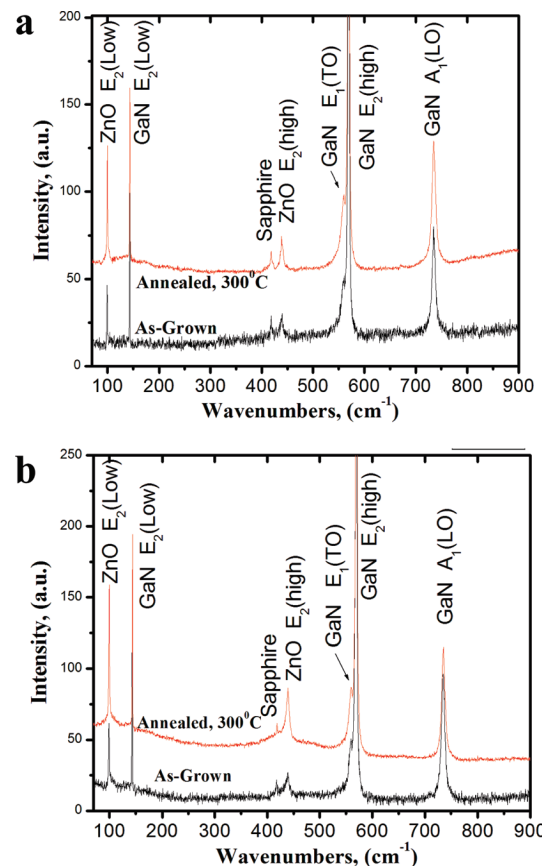


FIGURE 4. Effect of annealing at 300 °C on the micro-Raman spectra of epitaxial ZnO-NWs electrodeposited on *p*-GaN thin film. (a) Sample B (0.10 mM ZnCl₂) and (b) sample C (0.25 mM ZnCl₂).

ZnO films with fwhm values higher than 1.6° in that case, in spite of a single-crystal n-type GaN substrate of better quality (0.28° fwhm) (22).

The effects of ZnO deposition conditions and annealing on the heterojunction were characterized by micro-Raman experiments. The spectra in Figure 4 have been indexed with GaN and ZnO emission modes. For the samples B and C as-grown in 0.10 and 0.25 mM ZnCl₂ respectively (Figure 4a,b), the ZnO peaks were located at 100 and 439 cm⁻¹ and could be attributed to the low and high E_2 modes, respectively, of nonpolar optical phonons (38–41). Their fwhm were similar at 2 and 7.5 cm⁻¹ for the low and high E_2

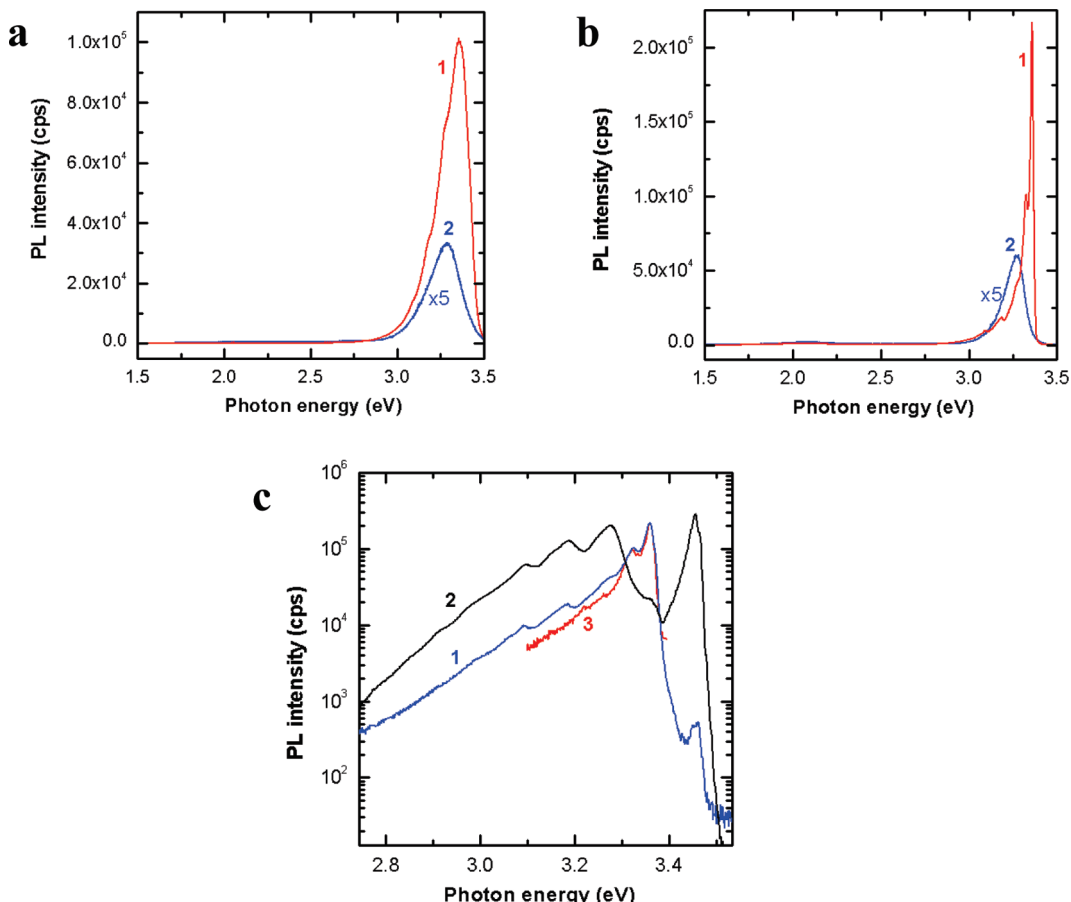


FIGURE 5. PL spectra under the excitation by the 325 nm line of a He–Cd laser of the epitaxial ZnO-NWs/p-GaN heterojunction: (a) as-grown sample B (0.10 mM ZnCl₂) and (b) sample B annealed at 300 °C. (Curves 1) measured at 10 K and (curves 2) at 300 K. (c) Near-bandgap PL spectra measured at 10K of a sample B (0.10 mM ZnCl₂) annealed at 300 °C (curve 1) and of the p-GaN substrate (curve 2). Curve 3 is the same as curve 1 but under excitation of the 363 nm line of an Ar laser.

modes, respectively. The thermal annealing treatment improved significantly the quality of the material because the peak intensity was increased by approximately a factor of 2 for the two samples investigated and the FWHMs were reduced to 1.5 and 6 cm⁻¹ for the low and high E_2 modes respectively. These latter values were comparable to those reported in the literature for very high quality ZnO (38, 39). In this work, the spectrum measurements were done with an incident light perpendicular to the top surface of the ZnO NW arrays on GaN substrate. According to Raman selection rules the $E_1(\text{TO})$ and $A_1(\text{TO})$ modes are forbidden when the incident light is parallel to the *c*-axis of NWs. In our studies, the absence of other phonon modes indicates that all NWs were perpendicularly oriented to the substrate surface. It can be concluded that ZnO nanowires were *c*-axis oriented, which is in agreement with the epitaxial growth of the ZnO material with the *c*-axis perpendicular to the substrate by XRD.

The emission properties of the nanostructured layers were characterized by photoluminescence (PL) measurements under UV excitation. At room temperature, the as-grown samples were dominated by a broad and asymmetric near-bandgap band with a maximum at 3.26 eV (382 nm) (Figure 5a). No significant visible PL-emission was found. The spectrum measured at 10K presented an UV-emission

intensity increased by more than 1 order of magnitude and the maximum wavelength of the emission was shifted to 3.36 eV. The intensity ratio between the UV and visible emissions of ZnO is a classical measure of the material quality because the visible emissions are due to point defects (36, 42–46). In the present case, the PL results demonstrate the very high quality and low point defect concentration in the as-electrodeposited material along with a significant quality improvement by the annealing treatment.

The shape of the near bandgap PL band is typical of highly doped ZnO samples (47–49). The broadening of the PL band involved was shown to be accounted for by the broadening of the band edges because of potential fluctuations induced by the high concentration of intrinsic defects or impurities. The width of the band tails, and the dependence of the full width at half-maximum (fwhm) of the PL band on carrier concentration can be calculated using the model for broadening of impurity bands in heavily doped semiconductors developed by Morgan (50). By using the established dependence of the fwhm of the PL band on carrier concentration and supposing that the model apply in the present case, we have estimated the electron concentration in our as-prepared sample B to be $4 \times 10^{20} \text{ cm}^{-3}$ and $5 \times 10^{20} \text{ cm}^{-3}$ at 10 K and at room temperature, respectively. The obtained values are likely overestimated because the model supposes

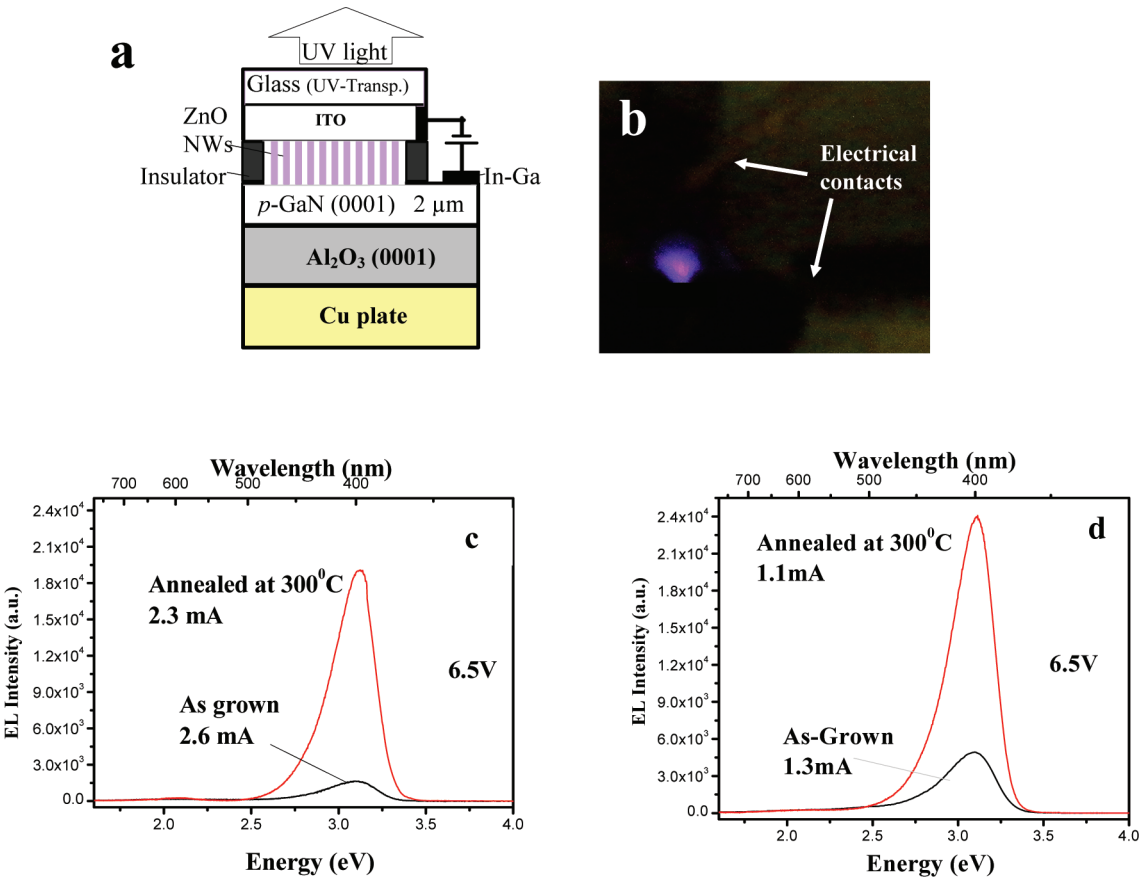


FIGURE 6. (a) Schematic of our ITO/ZnO-NWs/p-GaN/In–Ga heterojunction light emitting diode. (b) Image of the light spot emitted at room temperature under a forward bias of 6.5 V by a LED structure fabricated with an annealed sample B. (c) RT-EL spectra of the LED under 6.5 V bias for as-grown and thermal annealed samples B. (d) Same as (c) for sample C. (S devices 0.07 cm²).

that the broadening of the emission band is due to only heavy doping.

The narrowing of the near bandgap PL emission peak after annealing at 300 °C during 30 min in air can be explained by a decrease in electron concentration (16, 51). The emission intensity was also increased by a factor of 2 at both 300 and 10 K measuring temperatures (Figure 5b). A weak visible emission band around 2.1 eV was observed that can be assigned to interstitial oxygen (46). However, the intensity of this visible emission remained more than 2 orders of magnitude weaker than the UV one. In Figure 5c, the near band edge PL spectrum at 10 K of the annealed layer is compared to the spectrum of bare p-GaN substrate. A weak emission at 3.456 eV is observed on the bare GaN which is due to the recombination of acceptor bound excitons in the GaN substrate. Two PL bands at 3.360 and 3.324 eV are due to ZnO because they are not observed on bare GaN and under the excitation by the 363 nm (3.42 eV) line of an Ar laser. They are assigned to the recombination of neutral-donor bound excitons and donor–acceptor pairs in the ZnO nanowires, respectively. The bands at 3.277 eV, 3.185 eV, and 3.093 eV observed under the excitation by the 325 nm line of a He–Cd laser are due to the GaN substrate. The band at 3.277 eV is a zero-phonon line of the donor–acceptor pair recombination in the GaN substrate, while the lines at 3.185 eV, and 3.093 eV are the phonon replica with a LO phonon energy of 92 meV characteristic

for a GaN crystal with wurtzite structure. The lines at 3.277, 3.185, and 3.093 eV disappeared from the spectrum under the excitation by a 363 nm line of an Ar-laser (curve 3 in Figure 5c), since the excitation quantum energy was lower than the bandgap of GaN. When measured at room temperature, the GaN spectrum was characterized by a single emission peak located at 3.277 eV (378 nm). No blue emission due to a transition between the conduction band and deep Mg dopant levels was observed for the substrate (see Figure S2). In sample C (0.25 mM) (see Figure S3 in the Supporting Information), no emission from the GaN substrate was observed at 10 K, all the PL bands were related to the ZnO nanowires, and the near-band-edge emission due to ZnO was significantly higher than in the 0.1 mM sample. This is due to the higher density of the ZnO nanowires, and then a higher intensity of the emission arising from these nanowires.

The ZnO-NWs/p-GaN epitaxial heterostructures were integrated in the light-emitting diode device illustrated in the schematic of Figure 6a. The top of the ZnO wires was contacted with an ITO layer (Solems, France) deposited on a transparent glass sheet. The ITO layer acted as a transparent ohmic contact with ZnO (9). The top TCO (transparent conducting oxide) plate and the uncovered GaN layer were spaced by a thin insulator to avoid the direct contact between the two layers. The GaN layer was contacted with In–Ga eutectic. The device presented a rectifying current–

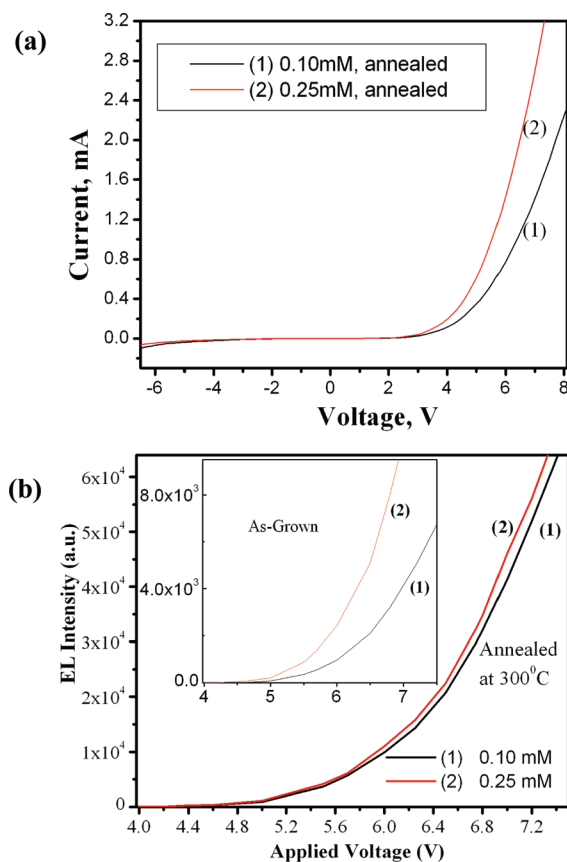


FIGURE 7. (a) Current–Voltage (*I*–*V*) characteristic curves of annealed n-ZnO NWs/p-GaN heterojunction diode curve (S device 0.07 cm²). (b) Room-temperature UV-electroluminescence intensity at 397 nm of the fabricated LED structure annealed at 300 °C as a function of the applied forward bias voltage. The inset shows the same curves for as-grown ZnO NWs/p-GaN heterojunctions.

voltage behavior with a turn-on forward bias voltage of about 3 V for annealed layers (Figure 7a). The diode current decreased after annealing (Figure 6c,d) in good agreement with the decrease in donor concentration (and then conductivity) that could be deduced from the excitonic PL emission narrowing in Figure 5. The LED electroluminescence spectra under a low forward bias voltage of 6.5 V are displayed in Figure 6c,d. The emission spectra of heterojunctions grown in 0.10 mM ZnCl₂ before and after annealing are dominated by a UV emission centered at 397 nm. The emission is shifted compared to the UV-PL peaks of ZnO (382 nm) and GaN (378 nm). The UV-emission can be assigned to the electron–hole radiative recombinations in ZnO and the redshift to some heating effects. The spectrum shows that the as-prepared heterojunction is of high quality and that electrochemical low temperature growth methods are very promising for the preparation of nanostructured active layers for solid-state UV-LED. However, the thermal annealing of ZnO/GaN structure dramatically increased the intensity of the EL without changing the emission peak wavelength. Annealing reduced the density of point defects in the ZnO and improved the quality of the ZnO surface and the ZnO/GaN interface. Similar EL spectra were found for the layer grown from 0.25 mM ZnCl₂ (Figure 6d). The EL intensity for the as-prepared heterojunction was significantly higher

showing a better quality of the ZnO material and of the interface. After annealing, the intensity remained slightly higher, probably due to the higher density of wires. The emission tail in the visible could be observed with the naked eyes above 5–6 V in the case of the annealed heterostructures (Figure 6b) and it was detected by the CCD camera above 4.4 V (threshold voltage), which is a very small value compared to literature data for ZnO (5–14). The devices were stable (52) and they could be operated at various voltages. Figure 7b shows the variation of the EL intensity with the applied forward bias of LED structure. It confirms the higher emission intensity from the layers as-grown at higher ZnCl₂ concentration (Figure 7b inset). The intensity was boosted after heterojunction annealing and the slightly better performance than of sample C compared to sample B was confirmed. The obtained results are remarkable in terms of the low voltage for the emission onset and of the purity of the UV-light produced by the devices because no significant parasitic visible-light contributions were measured. The reported results are all the more encouraging that the fabricated devices were not optimized for instance in terms of electrical contact between the ZnO-NWs and the ITO layer and light extraction in LEDs.

4. CONCLUSION

The growth by an electrochemical technique of ZnO nanowire arrays on a p-type GaN (0001) single crystal thin film supported on sapphire was demonstrated for the first time. The density of wires increased with the zinc precursor concentration. The wires were perfectly vertically oriented, directly attached to the GaN films and epitaxially grown. The epitaxial in-plane relationship was demonstrated to be ZnO(0001)[10̄10]||GaN(0001)[10̄10] by GA-XRD experiments. The epitaxy was of very good quality with a mosaicity of ZnO as low as 1.2°. The deposited ZnO NWs presented a very low density of intrinsic defects as demonstrated by micro-Raman and photoluminescence experiments. The only significant PL emission of the heterojunction at room temperature was the near-band-edge one of ZnO at 382 nm. After integration of the heterostructure in a light emitting diode structure, a rectifying behavior was found with a forward current onset at 3 V. The diodes emitted a single and bright UV light centered at 397 nm in the case of either as-prepared or annealed samples. The emission threshold voltage was very low at 4.4 V. The EL intensity increased rapidly with the applied voltage. After annealing, the violet-blue emission due to the long-wavelength tail could be easily observed with the naked eye above 5–6 V. The present results clearly state the remarkable quality of the electrochemical ZnO material and ZnO/p-GaN interface as well as effectiveness of electrodeposited epitaxial ZnO as an active layer in solid-state UV-LEDs. The performances of the fabricated devices were very high and encouraging since they were not optimized. The present work also paves the way for the fabrication of nano-UV-LED that may be obtained by addressing the ZnO NWs individually or in small groups.

Acknowledgment. Th.P. and B.V. are grateful to the C-nano Ile-de-France program (nanoZnO-LED Project) for funding O.L.'s postdoctoral fellowship and a part of this work. Stephan Borensztajn (LISE-UPR15, France) is acknowledged for SEM imaging of the samples.

Supporting Information Available: GA-XRD patterns and curve fits of the {2022}, {1122}, and {1012} families of plane; RT-PL of p-GaN and ZnO-NWs/p-GaN; effect of the temperature measurement between 10 and 300 K on the PL emission of annealed samples B and C; energy band diagram of the n-ZnO/p-GaN heterojunction (PDF). This material is available free of charge via the Internet at <http://pubs.acs.org>.

REFERENCES AND NOTES

- (1) Brown, H. E. *J. Phys. Chem. Solids* **1960**, *15*, 86.
- (2) Pauperté, T. Design of Solution-Grown ZnO Nanostructures. In *Toward Functional Nanomaterials*; Wang, Z. M., Ed.; Lecture Notes in Nanoscale Science and Technology; Springer: New York, 2009; Vol. 5, Chapter 2, pp 77–127.
- (3) Ozgur, U.; Alivov, Y. I.; Liu, C.; Teke, A.; Reschchikov, M. A.; Dogan, S.; Avrutin, V.; Cho, S. J.; Morkoc, H. *J. Appl. Phys.* **2005**, *98*, 041301.
- (4) Willander, M.; Yang, L. L.; Wadeasa, A.; Ali, S. U.; Asif, M. H.; Zhao, Q. X.; Nur, O. *J. Mater. Chem.* **2009**, *19*, 1006.
- (5) Zhang, X. M.; Lu, M. Y.; Zhang, Y.; Chen, L. J.; Wang, Z. L. *Adv. Mater.* **2009**, *21*, 2767.
- (6) Jeong, M. C.; Oh, B. Y.; Ham, M. H.; Myoung, F. *Appl. Phys. Lett.* **2006**, *88*, 202105.
- (7) Jeong, M. C.; Oh, B. Y.; Ham, M. H.; Lee, S. W.; Myoung, J. M. *Small* **2007**, *3*, 568.
- (8) Kim, D. C.; Han, W. S.; Kong, B. H.; Cho, H. K.; Hong, C. H. *Physica B* **2007**, *401–402*, 386.
- (9) Chen, C. H.; Chang, S. J.; Chang, S. P.; Li, M. J.; Chen, I. C.; Husueh, T. J.; Hsu, C. L. *Appl. Phys. Lett.* **2009**, *95*, 223101.
- (10) Park, W. I.; Yi, G. C. *Adv. Mater.* **2004**, *16*, 87.
- (11) Lee, S. D.; Kim, Y. S.; Yi, M. S.; Choi, J. Y.; Kim, S. M. *J. Phys. Chem. C* **2009**, *113*, 8954. S.
- (12) Kishwar, S.; Hasan, K.; Tzamalis, G.; Nur, O.; Willander, M.; Kwack, H. S.; Le Si Dang, D. *Phys. Status Solidi A* **2010**, *207*, 67.
- (13) Lai, E.; Kim, W.; Yang, P. D. *Nano Res.* **2008**, *1*, 123.
- (14) Ng, A. M. C.; Xi, Y. Y.; Hsu, Y. F.; Djurisic, A. B.; Chan, W. K.; Gwo, S.; Tam, H. L.; Cheah, K. W.; Fong, H. F.; Lui, H. F.; Surya, C. *Nanotechnology* **2009**, *20*, 445201.
- (15) Law, M.; Greene, L. E.; Johnson, J. C.; Saykally, R.; Yang, P. *Nat. Mater.* **2005**, *4*, 455.
- (16) Lupon, O.; Guérin, V. M.; Tiginyanu, I. M.; Ursaki, V. V.; Chow, L.; Heinrich, H.; Pauperté, T. *J. Photochem. Photobiol. A: Chem.* **2010**, *211*, 65.
- (17) Xu, C. K.; Shin, P.; Cao, L. L.; Gao, D. *J. Phys. Chem. C* **2010**, *114*, 125.
- (18) Barnes, T. M.; Olson, K.; Wolden, C. A. *Appl. Phys. Lett.* **2005**, *86*, 112112.
- (19) Lim, J. H.; Kang, C. K.; Kim, K. K.; Park, I. K.; Hwang, D. K.; Park, S. J. *Adv. Mater.* **2006**, *18*, 2720.
- (20) Fang, X.; Li, J. H.; Zhao, D. X.; Shen, D. Z.; Li, B. H.; Wang, X. H. *J. Phys. Chem. C* **2009**, *113*, 21208.
- (21) Pauperté, T.; Lincot, D. *Appl. Phys. Lett.* **1999**, *75*, 3817.
- (22) Pauperté, T.; Cortès, R.; Froment, M.; Beaumont, B.; Lincot, D. *Chem. Mater.* **2002**, *14*, 4702.
- (23) Pauperté, T.; Yoshida, T.; Cortès, R.; Froment, M.; Lincot, D. *J. Phys. Chem. B* **2003**, *107*, 10077.
- (24) Pauperté, T.; Lincot, D.; Viana, B.; Pellé, F. *Appl. Phys. Lett.* **2006**, *89*, 235112.
- (25) King, S. W.; Barnak, J. P.; Bremser, M. D.; Tracy, K. M.; Ronning, C.; Davis, R. F.; Nemanich, R. J. *J. Appl. Phys.* **1998**, *84*, 5248.
- (26) Uhlrich, J. J.; Grabow, L. C.; Mavrikakis, M.; Kuech, T. F. *J. Electron. Mater.* **2008**, *37*, 439.
- (27) Park, W. I.; Yi, G. C. *Adv. Mater.* **2004**, *16*, 87.
- (28) Lee, S. D.; Kim, Y. S.; Yi, M. S.; Choi, J. Y.; Kim, S. M. *J. Phys. Chem. C* **2009**, *113*, 8954. S.
- (29) Liu, R.; Vertegeel, A. A.; Bohannan, E. W.; Sorenson, T. A.; Switzer, J. A. *Chem. Mater.* **2001**, *13*, 508.
- (30) Limmer, S. J.; Kulp, E. A.; Switzer, J. A. *Langmuir* **2006**, *25*, 10535.
- (31) Elbelghiti, H.; Pauperté, T.; Lincot, D. *Phys. Status Solidi A* **2008**, *205*, 2360.
- (32) Goux, A.; Pauperté, T.; Lincot, D. *Electrochim. Acta* **2006**, *51*, 3168.
- (33) De Tacconi, N.; Chenthamarakshan, C. R.; Rajeshwar, K.; Pauperté, T.; Lincot, D. *Electrochim. Commun.* **2003**, *5*, 220.
- (34) Goux, A.; Pauperté, T.; Chivot, J.; Lincot, D. *Electrochim. Acta* **2005**, *50*, 2239.
- (35) Pauperté, T.; Bataille, G.; Joulaud, L.; Vermersch, J. F. *J. Phys. Chem. C* **2010**, *114*, 194.
- (36) Pauperté, T.; Jouanno, E.; Pellé, F.; Viana, B.; Ashehoun, P. *J. Phys. Chem. C* **2009**, *113*, 10422.
- (37) Perriere, J.; Million, E.; Seiler, W.; Boulmer-Leborgne, C.; Craciun, V.; Albert, O.; Loulergue, J. C.; Etchepare, J. *J. Appl. Phys.* **2002**, *91*, 690.
- (38) Lupon, O.; Chow, L.; Chai, G.; Heinrich, H. *Chem. Phys. Lett.* **2008**, *465*, 249.
- (39) Lupon, O.; Ursaki, V. V.; Chai, G.; Chow, L.; Emelchenko, G. A.; Tiginyanu, I. M.; Gruzintsev, A. N.; Redkin, A. N. *Sens. Actuators, B* **2010**, *144* (1), 56.
- (40) Zhang, Y.; Jia, H. B.; Wang, R. M.; Chen, C. P.; Luo, X. H.; Yu, D. P.; Lee, C. J. *Appl. Phys. Lett.* **2003**, *83*, 4631.
- (41) Cheng, H. M.; Hsu, H. C.; Tseng, Y. K.; Lin, L. J.; Hsieh, W. F. *J. Phys. Chem. B* **2005**, *109*, 8749.
- (42) Chen, Y.; Bagnall, D. M.; Koh, H. J.; Park, K. T.; Hiraga, K.; Zhu, Z.; Yao, T. *J. Appl. Phys.* **1998**, *84*, 3912.
- (43) Vanheusden, K.; Warren, W. L.; Seager, C. H.; Tallant, D. R.; Voigt, J. A.; Gnade, B. E. *J. Appl. Phys.* **1996**, *79*, 7983.
- (44) Lin, B.; Fu, Z.; Jia, Y. *Appl. Phys. Lett.* **2001**, *79*, 943.
- (45) Xu, P. S.; Sun, Y. M.; Shi, C. S.; Xu, F. Q.; Pan, H. B. *Nucl. Instrum. Methods Phys. Res., Sect. B* **2003**, *199*, 286.
- (46) Ahn, C. H.; Kim, Y. Y.; Kim, D. C.; Mohanta, S. K.; Cho, H. K. *J. Appl. Phys.* **2009**, *105*, 013502.
- (47) Ursaki, V. V.; Tiginyanu, I. M.; Zalamai, V. V.; Rusu, E. V.; Emelchenko, G. A.; Masalov, V. M.; Samarov, E. N. *Phys. Rev. B* **2004**, *70*, 155204.
- (48) Zalamai, V. V.; Ursaki, V. V.; Rusu, E. V.; Arabadji, P.; Tiginyanu, I. M.; Sirbu, L. *Appl. Phys. Lett.* **2004**, *84*, 5168.
- (49) Iliopoulos, E.; Doppelopudi, D.; Ng, H. M.; Moustakas, T. D. *Appl. Phys. Lett.* **1998**, *73*, 375.
- (50) Morgan, T. N. *Phys. Rev.* **1965**, *139*, A343.
- (51) Lupon, O.; Pauperté, T.; Chow, L.; Viana, B.; Pellé, F.; Roldan Cuenya, B.; Ono, L. K.; Heinrich, H. *Appl. Surf. Sci.* **2010**, *256*, 1895.
- (52) Lupon, O.; Pauperté, T.; Viana, B. *Adv. Mater.* **2010**, DOI: 10.1012/adma.201000611.

AM100334C